

## **LEFM PREDICTION AND REPAIR STRATEGY FOR CRACK EXTENSION DUE TO CORROSION OF REINFORCEMENT**

M. Ohtsu

Department of Architecture and Civil Engineering, Kumamoto  
University, Kumamoto, Japan

S. Yoshimura

Kajima Corporation, Ltd. Kyushu Branch, Fukuoka, Japan

### **Abstract**

In order to repair cracks of concrete, the causes of cracking have been intensively studied and can be identified mostly in inspected structures. One of critical cracks is known to result from corrosion of steel reinforcement in concrete. Due to expansion of corrosive products, tensile cracks of various patterns are nucleated around rebars. Initiation and extension of these cracks are studied experimentally by electrolytic corrosion tests. To clarify crack-nucleating mechanisms, numerical analysis by the boundary element method (BEM) is conducted, on the basis of the linear elastic fracture mechanics (LEFM). The analyses of stress distribution and crack traces are performed. From these results, strategy by means of fiber-reinforced concrete is discussed for repairing cracks due to corrosion of rebars.

Key words : Cracking due to Corrosion of Rebar, Boundary Element Method, Linear Elastic Fracture Mechanics, Fiber Reinforced Concrete

## 1 Introduction

It is so often to find out cracks in concrete structures that the causes of cracking have been studied intensively. One of critical cracks result from corrosion of steel reinforcement in concrete. Corrosion of rebars is an inherent problem of reinforced concrete (RC) structures subjected to severe chloride attack. Because corrosive products expand the area of the reinforcement, high tensile stress is generated in concrete and thus tensile cracks are nucleated.

In order to analyze crack extension in concrete, numerical modeling based on fracture mechanics has been well developed (Ingraffea and Saouma; 1985). Chahrour and Ohtsu (1994) applied a discrete crack model based on the linear elastic fracture mechanics (LEFM) and the boundary element method (BEM) successfully to predict crack growth in concrete. Further, Ohtsu and Yoshimura (1997) have analytically clarified nucleating mechanisms of various crack patterns, assuming pressure distribution due to the expansion of corrosive products. In the present paper, initiation and extension of cracks are observed in experiments. For these cracks, the nucleating mechanisms are analytically investigated, and then repair strategy by means of fiber-reinforced concrete is discussed.

## 2 Experiments

### 2.1 Concrete and RC specimen

Specimens were made of normal concrete and steel-fiber reinforced (SFR) concrete. Mixture proportions of concrete are listed in Table 1. The water-cement ratio by weight (W/C) and the volume ratio of fine

Table 1 Mixture proportions of concrete

concrete	W/C (%)	s/a (%)	weight per volume (kg/m <sup>3</sup> )				
			W	C	S	G	fiber
normal	45	42	172	378	719	1122	-
steel fiber reinforced	45	42	223	495	611	954	78

Table 2 Mechanical properties of concrete at 28 days

concrete	compressive strength (MPa)	tensile strength (MPa)	Young's modulus (GPa)	Poisson's ratio
normal	54.9	3.96	35.2	0.22
steel fiber reinforced	56.1	4.26	33.3	0.25

aggregate (s/a) are common in both mixtures. The maximum gravel size is 20 mm. For SFR concrete, steel fibers of 30 mm length are mixed as 1 % volume ratio. To keep the slump value around 6 cm by mixing, air-entrained admixture is added. Mechanical properties of concrete at the age of 28 days are summarized in Table 2. These Young's moduli and Poisson's ratios are employed in the BEM analysis.

Configuration of the specimen is shown in Fig. 1. Two specimens of dimensions 10 cm x 25 cm x 40 cm were made of normal concrete and SFR concrete. Four rebars were embedded vertically to the specimen,

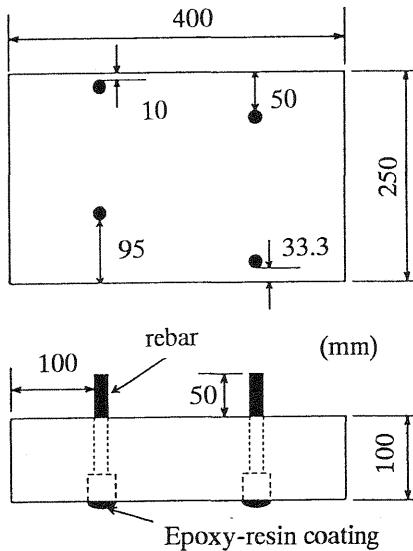


Fig. 1 Sketch of the specimen.

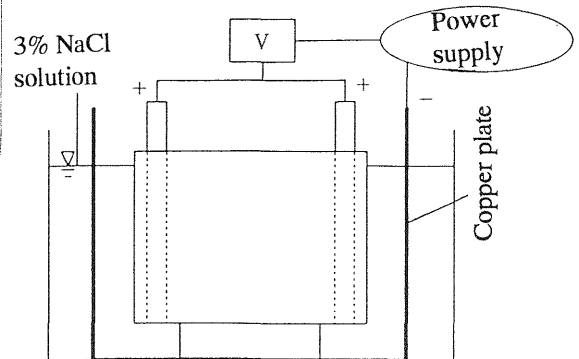


Fig. 2 Electrolytic corrosion test.

varying cover thickness  $T_p$  as 10 mm, 33.3 mm, 50 mm, and 95 mm. Each rebar was a deformed bar of nominal 10 mm diameter (D10). The specimens were moisture-cured for 28 days in the standard room (20°C). To protect from corrosion, the shaded zones of the rebars in Fig. 1 were coated with epoxy-resin. To let the rebars corroded acceleratedly, an electrolytic corrosion test was conducted. As shown in Fig. 2, a copper plate was placed in a tub which was filled with 3% NaCl solution. Between the rebars and the copper plate, 200 mA electric current was charged until cracks were visually observed at the surface.

## 2.2 Crack patterns

Typical crack patterns observed after the tests are shown in Fig. 3. Rectangles in the figure represent locations of strain gauges to detect cracking. In the case of shallow cover thickness ( $T_p=10$  mm), a spalling crack is observed in normal concrete. Both a spalling crack and a surface crack are observed in the case  $T_p=33.3$  mm of normal concrete. Such cracks were effectively arrested in SFR concrete. In the case  $T_p=50$  mm, an internal crack (labelled 2) and a diagonal crack (labelled 3) are observed in normal concrete, following the surface crack (labelled

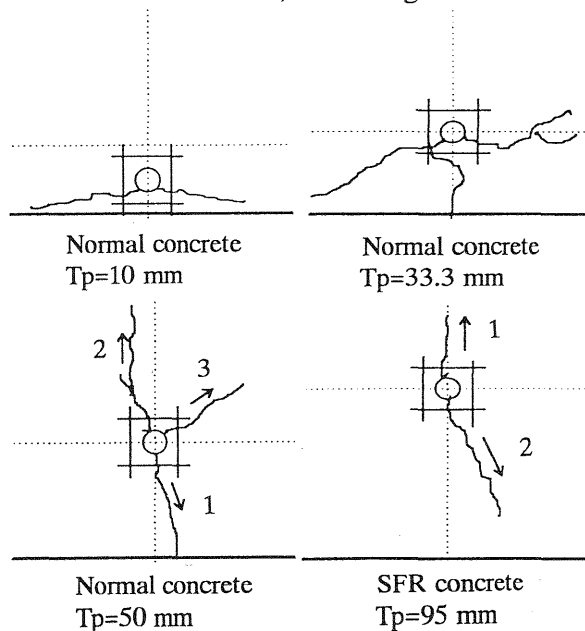


Fig. 3 Crack patterns observed.

1). In contrast, the internal crack was always observed first in SFR concrete. The case  $T_p=95$  mm is given in the figure. A surface crack

(labelled 2) is observed after extension of an internal crack (labelled 1).

As reported by Matsushima et al. (1994), crack patterns are associated with the ratio  $D/d$ , where  $D=2T_p + d$  and  $d$  is the diameter of the rebar. In the case  $D/d < 3.0$ , the spalling crack is primarily observed. In the other case, the surface crack propagates. According to the results in Fig. 3, the cases  $T_p=10$  mm, 33.3 mm, 50 mm, and 95 mm correspond to those of  $D/d= 3, 7.63, 11, \text{ and } 20$ , respectively. The criterion is available for normal concrete, whereas the cracking process of SFR concrete seems slightly different from that of normal concrete.

Previous experiments by Ohtsu et al.(1995) demonstrated other cracks than the surface crack could be nucleated either by following it or in the case of the surface crack being arrested by aggregate. According to the stress analysis by Ohtsu and Yoshimura (1997), the spalling crack and/or the diagonal crack could follow the surface crack due to hydrostatic expansion of corrosive products. With the increase of lateral expansion, the internal crack could follow the surface crack.

Taking into account these findings, the cracking mechanisms of the cases shown in Fig. 3 are investigated analytically.

### 3 BEM analysis

#### 3.1 Mixed-mode failure

The criterion for crack extension to an arbitrary direction is derived from the criterion of the maximum circumferential stress by Erdogan and Sih (1963). In the case that a new crack is nucleated from the tip of a pre-existing crack with the angle  $\theta$ ,

$$K_I \sin\theta + K_{II}(3\cos\theta - 1) = 0, \quad (1)$$

$$\cos(\theta/2)[K_I \cos^2(\theta/2) - 3/2 K_{II} \sin\theta] = K_{IC}, \quad (2)$$

where  $K_I$  and  $K_{II}$  are the stress intensity factors of mode I and mode II, respectively.  $K_{IC}$  is the critical stress intensity factors of concrete. In the present analysis,  $K_{IC}$  is 0.725 MPa  $m^{0.5}$  which was determined experimentally by Ohtsu and Yoshimura (1997). Even in the case of SFR concrete, the same value was assumed in the analysis because the critical stress intensity factor of SFR concrete was neither easily defined

nor readily determined from the experiment.

In the BEM analysis, the differential equations of the plane-strain state and of the elastostatics are converted into the integral form on the boundary. The boundary is digitized and the boundary conditions are taken only into consideration. Crack extension is easily modeled, creating just new boundary meshes. After solving integral equations in respect to tractions and displacements on the boundary, stresses at arbitrary locations can be determined. The stress intensity factors  $K_I$  and  $K_{II}$  are computed from the displacements at the crack-tip elements by using Smith's formulation (Smith and Mason; 1982).

### 3.2 BEM model

#### 3.2.1 Two-domain model

To analyze extension of the spalling crack, two-domain BEM by Chahrour and Ohtsu (1992) is applied. A model is given in Fig. 4. A semi-circle of 5 mm diameter represents location of the rebar where expanding pressure due to corrosive products is applied. All elements are 2.5 mm long. Along the interface boundary which is a linear approximation of the actual crack in Fig. 3, two domains are stitched.

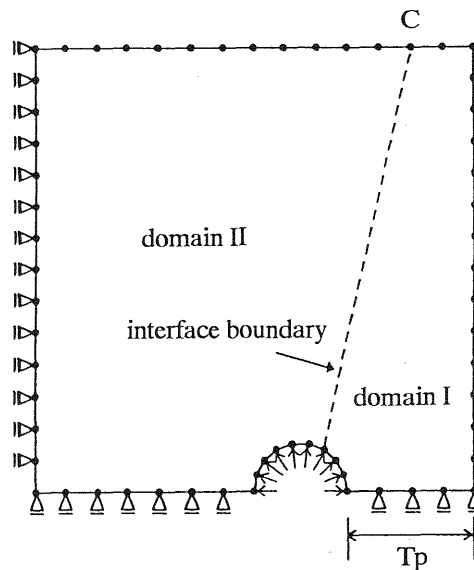


Fig. 4 Two-domain model.

At each step of the analysis, the stress intensity factors at the crack tip are computed. The crack tip corresponds to the lower end of the interface boundary in the figure. The direction  $\theta$  of crack extension is determined by eq. 1 and the pressure level corresponding to the critical intensity factor  $K_{IC}$  is obtained from eq. 2. Then two crack elements are newly put forth in the direction  $\theta$  at the crack tip, generating new boundaries in both domains I and II. The new elements are connected at a new crack tip and a new interface boundary is created, linearly connecting the crack tip with the termination point C in the figure. Thus, the direction of a new crack and the location of a crack tip are automatically assigned.

### 3.2.2 One-domain model

To analyze the extension of a surface crack and an internal crack, a semi-infinite model is considered. The model is illustrated in Fig. 5.

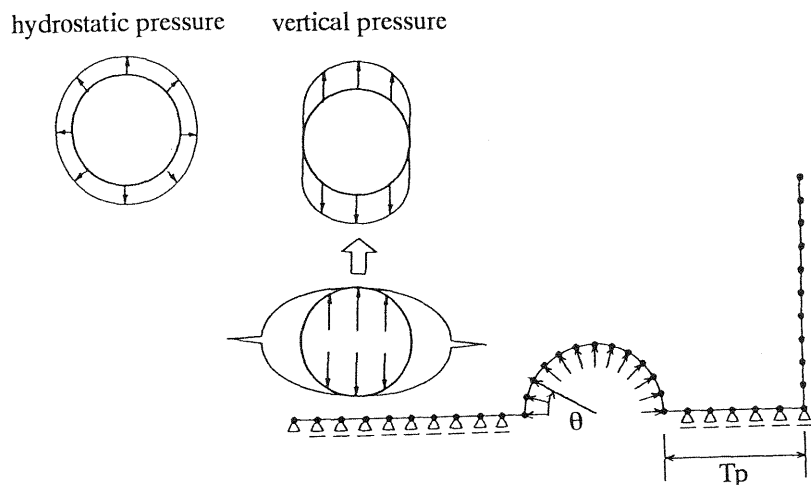


Fig. 5 One-domain model.

The symmetric axis of the concrete block is replaced by the crack-extension boundary at the bottom. To simulate crack extension, the displacement constraint at the bottom boundary in Fig. 5 is released. In eqs. 1 and 2, the model leads to the case that  $\theta = 0$  and  $K_{II} = 0$ . Accordingly, the crack extends if  $K_I > K_{IC}$ . In the case that a surface crack propagates toward a stress-free surface, the nodes on the boundary

$T_p$  are disconnected one by one. An internal crack, in the other case, extends inside from the semi-circular boundary of the reinforcement. The length of the stress-free surface is taken as 10 cm. All boundary meshes are 2 mm long and the points where stresses are estimated are located 1mm radially apart from the semi-circular boundary.

### 3.2.3 Expansive pressure

Because distribution of actual expansive pressure is not known, two kinds of pressure distribution are taken into consideration to simulate the expansion of corrosive products. These are also shown in Fig. 5. One is hydrostatic radial pressure and the other is vertical expansion pressure by neglecting horizontal pressure of the hydrostatic. The vertical pressure distribution is taken into account, based on the fact that due to nucleation of small tensile cracks the contact between the reinforcement and concrete might be broken as shown in the figure.

## 4 Results and discussion

### 4.1 Spalling crack

The cases of spalling cracks shown in Fig. 3 ( $T_p=10$  mm and  $T_p=33.3$  mm of normal concrete) were analyzed by using the two-domain BEM model in Fig. 4. The initial interface boundary was taken linearly, approximating a spalling crack observed in the test. Crack traces analyzed are compared with those of actual cracks in Fig. 6. The effect of expansive pressure is clearly observed. In the case  $T_p=10$  mm, crack trace due to vertical pressure is in better agreement with actual crack trace than that of hydrostatic pressure. In the case of  $T_p=33.3$  mm, it seems that extension of the spalling crack is governed by the vertical pressure, while the subsequent surface crack might be generated due to hydrostatic pressure. These results imply that the dominant action which generates the spalling crack is vertical pressure due to corrosive expansion. As reported by Ohtsu et al. (1995) previously, it is noted that the spalling crack could be nucleated in only the case that the surface crack is arrested by aggregate and other inclusions. The fact was also confirmed by rebar corrosion in SFR concrete, because neither the surface crack nor the spalling crack was not observed visually in the case of shallow cover thickness.

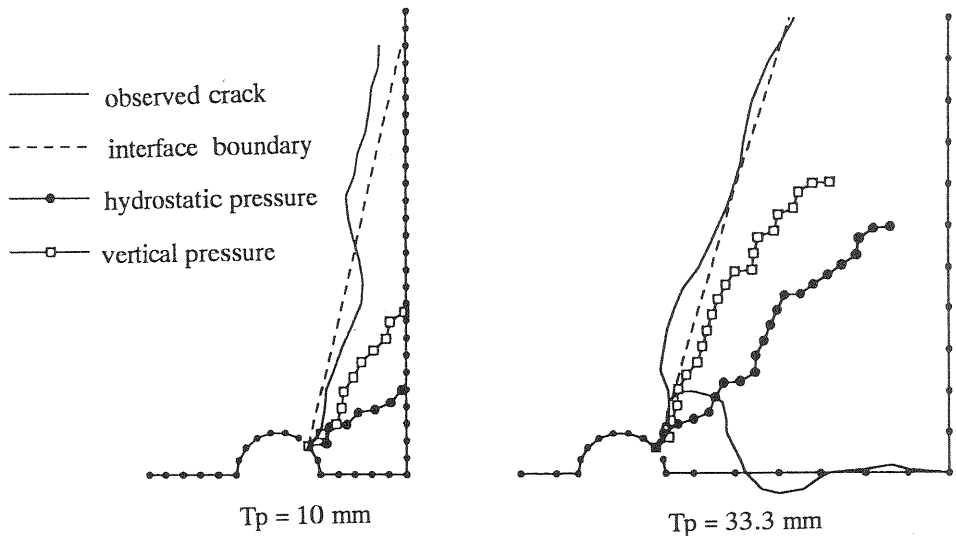


Fig. 6 Crack traces of the spalling cracks by the two-domain BEM.

#### 4.2 Surface crack

The case where the surface crack propagates toward the stress-free surface ( $T_p=50$  mm of normal concrete in Fig. 3) was analyzed by using the one-domain BEM model in Fig. 5. As seen in Fig. 3, the internal crack is nucleated following the surface crack, and then the diagonal crack propagates. A relation between the expansive pressure and the vertical displacement at the crown of the semi-circle ( $\theta=90^\circ$  in Fig. 5) is shown in Fig. 7 (a). Under hydrostatic pressure, the peak pressure is observed at point A where in the analysis a surface crack starts to propagate. Stress distribution at 1 mm apart from the semi-circle boundary is given in Fig. 7(b) at three pressure levels A, B, and C. These are indicated in Fig. 7 (a). Circumferential tensile stresses are plotted against the angle  $\theta$  shown in Fig. 5. At the pressure level A, the peak stress is observed in the direction of  $135^\circ$ , which must be associated with the initiation of a spalling crack. At the pressure level B, another peak stress is found around  $45^\circ$ , which could explain nucleation of a diagonal crack. The actual crack trace in Fig. 3, however, is not coincident with these findings.

The case of vertical pressure is shown in Fig. 8. The peak pressure is

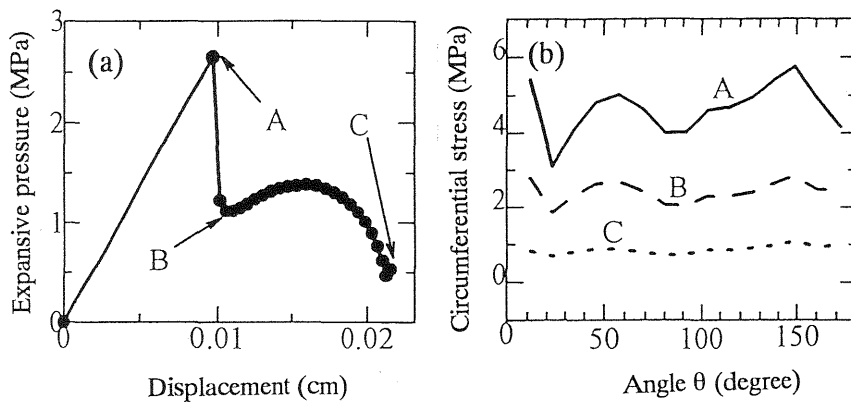


Fig. 7 (a) Pressure versus vertical displacement at the crown due to hydrostatic pressure and (b) stress distribution around the hole of reinforcement under extension of the surface crack.

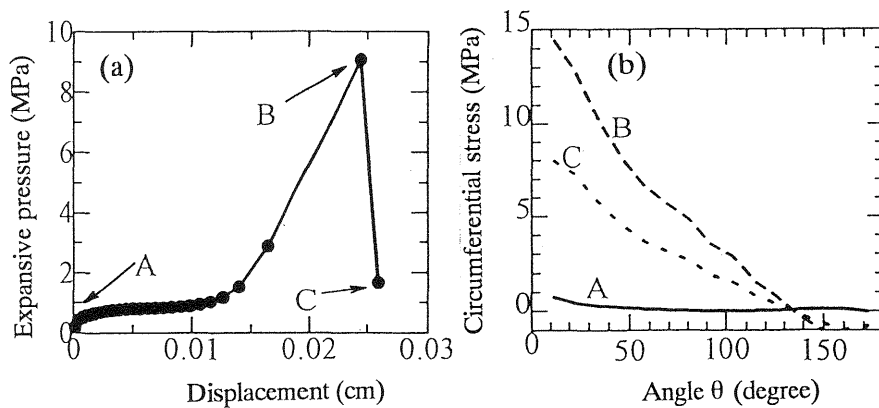


Fig. 8 (a) Pressure versus vertical displacement at the crown due to vertical pressure and (b) stress distribution around the hole of reinforcement under extension of the surface crack.

reached at point B after gradual increase from the point A, although a surface crack starts to propagate at the pressure level A. The stress distribution in Fig. 8 (b) shows high stress zone around  $0^\circ$  in any pressure levels. Thus, a possible initiation of the internal crack is suggested, which is in good agreement with the crack trace in Fig. 3.

### 4.3 Internal crack

The case that an internal crack propagates toward the inside was analyzed, corresponding the crack trace  $T_p=95$  mm in Fig. 3. The case of hydrostatic pressure was quite similar to Fig. 7, suggesting only initiation of a spalling crack. This is not the case of experimental observation.

The case of vertical pressure was analyzed and results are given in Fig. 9. At pressure level at A, an internal crack begins to propagate. With increase of the pressure, new high-stress zone is created around 180° direction. This results in the initiation of the surface crack, represented by the crack trace in Fig. 3.

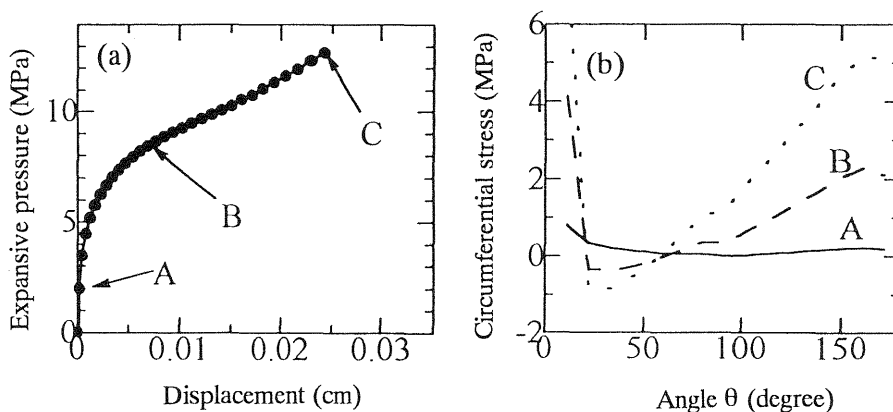


Fig. 9 (a) Pressure versus vertical displacement at the crown due to vertical pressure and (b) stress distribution around the hole of reinforcement under extension of the internal crack.

## 5 Repair strategy

The initiation of cracks due to the expansion of corrosive products is studied by the BEM analysis based on the LEFM. Based on the results, the following strategy for repairing is proposed.

(1) A surface crack is nucleated due to stress concentration at the closest zone of concrete to the stress-free surface. But, this crack is readily arrested by aggregate and other inclusions. In the case that the surface crack is arrested, a spalling crack is generated. For both cracks, the use of SFR concrete is quite effective.

(2) When a surface crack starts to extend in normal concrete, the stress

distribution suggests the initiation of an internal crack. Thus, in concrete structures on demand for long service life, cracks inside the reinforcement is to be inspected when the surface cracks are found.

(3) In the case that an internal crack propagates toward the inside in SFR concrete, a surface crack could follow the internal crack. It implies that the whole region around the reinforcement should be repaired in the case that the surface cracks are observed in SFR concrete.

## References

- Chahrouh, A. H. and Ohtsu, M.(1992) Multi-Domain BEM Implementation for Mixed-Mode Cracking in Concrete, **Fracture and damage of Concrete and Rock (FDCR-2)**, E & FN Spon, London, 196-205.
- Chahrouh, A. H. and Ohtsu, M.(1994) Crack Growth Prediction in Scaled Down Model of Concrete Gravity Dam, **Theoretical and Applied Fracture Mechanics**, 21, 29-40.
- Erdogan, F and Sih, G. C. (1963) On the Crack Extension in Plates under Plane Loading and Transverse Shear, **Journal of Basic Eng.**, 12, 519-527.
- Ingraffea, A. R. and Saouma, V.(1985) Numerical Modeling of Discrete Crack Propagation in Reinforced and Plain Concrete, **Fracture Mechanics of Concrete**, Martinus Nijhoff Publishers, Dordrecht, 171-225.
- Matsushima, M., Tsutumi, T., Seki, H. and Matsui, K. (1994) Design of Cover Thickness for Reinforced Concrete Structures subjected to Severe Salt Attack, **Proc. of Japan Society of Civil Engineers**, 490/V-23, 41-49.
- Ohtsu, M., Tutumi, T., Murakami, Y. and Kudo, Y.(1995) Analytical and Experimental Study on Crack Propagation due to Rebar Corrosion, **Proc. Japan Concrete Institute**, 17(1), 955-960.
- Ohtsu, M. and Yoshimura, S. (1997) Analysis of Crack Propagation and Crack Initiation due to Corrosion of Reinforcement, **Construction and Building Materials**, 11(7-8), 437-442.
- Smith, R. N. L. and Mason, J. C. (1982) A Boundary Element Method for Curved Crack Problem in Two-Dimensions, **Boundary Element Methods in Engineering**, Springer, London, 472-484.